PHYSICAL REVIEW D VOLUME 43, NUMBER 8 15 APRIL 1991

Optimization of laser interferometers for the detection of gravitational waves from coalescing binaries

A. Krolak
Institute of Mathematics, Polish Academy of Sciences, Warsaw, Poland.

J. A. Lobo
Grup de Relativitat de l'IEC and Departament de Física Fonamental, Universitat de Barcelona, Barcelona, Spain

B. J. Meers
Department of Physics and Astronomy, University of Glasgow, Glasgow G12 8QQ, Scotland, United Kingdom
(Received 6 September 1990)

Coalescing compact binary systems are important sources of gravitational waves. Here we investigate the detectability of this gravitational radiation by the recently proposed laser interferometers. The spectral density of noise for various practicable configurations of the detector is also reviewed. This includes laser interferometers with delay lines and Fabry-Pérot cavities in the arms, both in standard and dual recycling arrangements. The sensitivity of the detector in all those configurations is presented graphically and the signal-to-noise ratio is calculated numerically. For all configurations we find values of the detector's parameters which maximize the detectability of coalescing binaries, the discussion comprising Newtonian- as well as post-Newtonian-order effects. Contour plots of the signal-to-noise ratio are also presented in certain parameter domains which illustrate the interferometer's response to coalescing binary signals.

I. INTRODUCTION

Long-base-line laser interferometers are currently being proposed for the detection of gravitational waves by a number of experimental groups—see Ref. 1 for a review. The optics of the interferometers may be arranged in various ways: Both delay lines and cavities may be used with either standard, detuned, dual or resonant cycling.[2–4] This enables the spectral density of noise in the interferometer to be optimized according to the gravitational signal to be detected.

Recently, one of us has derived a single formula describing the frequency response of a gravitational-wave detector which is valid whether the interferometer contains delay lines or cavities, whether or not recycling is used, and whether the recycling arrangement is standard, detuned, or dual.[5] In this paper we shall discuss the detectability of an important source of gravitational waves recently discussed in the literature: coalescence of binary-star systems consisting of neutron stars or black holes.[6] With the aid of the formula just mentioned, we calculate numerically the signal-to-noise ratio that can be achieved with an optimum filtering of the data for the possible optical configurations of the interferometer. We also determine the parameters that maximize such signal-to-noise ratio for each optical configuration. We do not discuss explicitly the case of detuned recycling since this arrangement has already been investigated;[7] furthermore, dual recycling is both more flexible and gives better performance.

The plan of the paper is as follows. In Sec. II we summarize the derivation of the general transfer function of the laser interferometer applicable to all configurations of the instrument and we give the spectral density of the photon-counting noise. We assume that this will be the dominant noise in the planned long-base-line interferometer for frequencies above 100 Hz. In Sec. III we give approximate analytical formulas for spectral densities of noise for various configurations of the detector. In Sec. IV we give the numerical analysis of the sensitivity (inverse of the spectral density) of the detector. In Sec. V we briefly review the problem of detection of coalescing binaries with optimal filtering. We evaluate numerically signal-to-noise ratios for all optical arrangements of the detector. We find the optimum values for various parameters of the antenna: reflectivities and transmissions of mirrors, tunings of cavities, and number of bounces in the delay lines. We present our results on a series of contour plots so that the signal-to-noise ratio for any detector can be read off. In Sec. VI we discuss the implications of these results for the detection of coalescing binaries and make a few concluding remarks. Numerical values of the parameters of the detector apply to the proposed joint German-British interferometric gravitational-wave detector.[8]

II. FREQUENCY RESPONSE OF INTERFEROMETRIC GRAVITATIONAL-WAVE DETECTORS

The basic optical arrangement of these systems is shown in Fig. 1. A suitably polarized gravitational wave induces opposite length changes in the two arms of the interferometer, producing phase shifts on the sensing light which are converted into intensity changes by interference at the beam splitter. These intensity changes

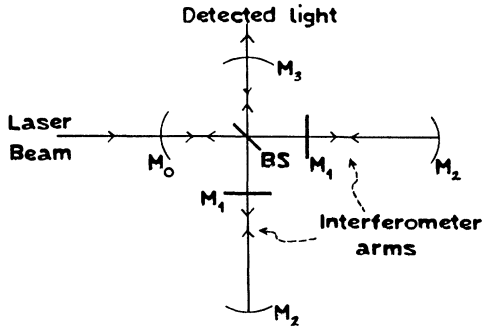

FIG. 1. Optical arrangement of an interferometric gravitational-wave detector. The Michelson interferometer detects induced phase differences, which are made larger by the multiple-bounce system formed between mirrors M_1 and M_2. Standard recycling places mirror M_0 to recycle the laser power, while dual recycling adds M_3 to recycle signal sidebands.

constitute the gravitational-wave signal.

We shall consider a single Fourier component of a gravitational wave, which we will regard as phase modulating the light to give two sidebands. The interferometer is arranged so that when the light beams from the two arms meet at the beam splitter, the original laser frequency heads back to mirror M_0, while any sidebands produced by differential phase modulation travel toward mirror M_3 and the output of the interferometer. The mirrors M_0 and M_3 will, in general, have different relative positions and reflectivities which must be taken into account when calculating how both laser light and sidebands resonate. So the sideband amplitude emerging from the output mirror may be found if we regard the optical system as consisting of a split cavity, in which the laser frequency and sidebands experience different reflectivities and optical lengths. The signal in this case is just the emerging from an equivalent single cavity with (composite) input mirror M_1, and end mirror M_2, length L. The input mirror has amplitude reflection and transmission coefficients R_{1c}, T_{1c} for the carrier (laser frequency) and R_{1s}, T_{1s} for the two sidebands (we will only consider the usual case of $R_{1+}=R_{1-}$). The end mirror has reflectance R_2 for all frequencies. It is the interpretation of R_{1c}, R_{1s}, etc., that determines the optical system to which the results apply.

For a simple delay line system with no recycling $R_{1c}=R_{1s}=0$, R_2 is the reflectivity of the whole delay line and L must be regarded as the optical length of the delay line. If there are N reflections in the delay line, then L is approximately N times the physical length l of each arm of the interferometer. If standard recycling is used, the carrier reflectivity R_{1c} is just equal to the reflectivity of the recycling mirror M_0, while in dual recycling it is M_3 that determines the sideband reflectivity R_{1s}.

In a cavity system, R_2 is just the reflectivity of the end mirror and L is the length of the cavity. With no recycling, R_1 is frequency independent—it is simply the reflectivity of the cavity input mirror. In standard and detuned recycling, R_{1c} is determined by the combination of M_0 and M_1, which form a cavity. In dual recycling, R_{1s} is determined by the combination of M_1 and the output mirror M_3.

Let us consider a gravitational wave of optimum polarization, amplitude $h_0\cos\omega t$, incident on the antenna. In order to calculate the effect that this has on the light in our equivalent cavity, we will regard the light as being the sum of many beams, each of which has experienced a different number of reflections in the cavity. We will first determine the influence of the gravitational wave on one beam, then add the contributions from all the beams.

If the transit time of one beam is τ, the differential phase shift $\delta\phi$ induced on the light in one round trip is

$$\delta\phi=\int_{t-\tau}^{t}\omega_L h_0\cos\omega t\,dt=\frac{h_0\omega_L}{\omega}\sin\left[\frac{\omega\tau}{2}\right]\left[e^{i\omega(t-\tau/2)}+e^{-i\omega(t-\tau/2)}\right], \tag{2.1}$$

where we have used the exponential representation of $\cos\omega t$ and ω_L is the angular frequency of the light. The effect of this phase shift is to multiply the field by $e^{i\delta\phi}\approx 1+i\delta\phi$ producing a sideband-field offset by $\pm\omega$ from the laser frequency. The total sideband field is found by adding the contributions generated in each bounce; taking just the $+\omega$ field E_+ emerging from the cavity,

$$\frac{E_+}{E_0}=iT_{1c}T_{1s}R_2\frac{h_0\omega_L}{\omega}\sin\left[\frac{\omega\tau}{2}\right]e^{i\omega(t-\tau/2)}\sum_{N=1}^{\infty}(R_{1c}R_2)^{N-1}e^{iN\delta_c}\sum_{n=1}^{\infty}(R_{1s}R_2e^{-i\omega\tau})^{n-1}e^{in\delta_c}, \tag{2.2}$$

where E_0 is the incident laser field and δ is the phase offset of the cavity from resonance: δ_c is that for the carrier, δ_s that for the sidebands. The $e^{-in\omega\tau}$ term reflects the change in phase of the signal over the history of the light stored in the cavity. Summing the series gives

$$\frac{E_+}{E_0}=\frac{iT_{1c}T_{1s}R_2h_0\omega_L\sin(\omega\tau/2)e^{i\omega(t+\tau/2)}e^{i(\delta_c+\delta_s-\omega\tau)}}{\omega(1-R_{1c}R_2e^{i\delta_c})(1-R_{1s}R_2e^{i(\delta_s-\omega\tau)})}, \tag{2.3}$$

which may be rewritten as

$$\frac{E_+}{E_0}=\frac{iT_{1c}T_{1s}R_2h_0\omega_L\sin(\omega\tau/2)e^{i\omega(t+\tau/2)}}{\omega(1-R_{1c}R_2)^2(1-R_{2s}R_2)^2}\frac{(e^{i\delta_c}-R_{1c}R_2)(e^{i(\delta_s-\omega\tau)}-R_{1s}R_2)}{(1+F_c'\sin^2\delta_c/2)\{1+F_s'\sin^2[(\delta_s-\omega\tau)/2]\}}\ , \tag{2.4}$$

where

$$F_c'=\frac{4R_{1c}R_2}{(1-R_{1c}R_2)^2},\quad F_s'=\frac{4F_s^2}{\pi^2}=\frac{4R_{1s}R_2}{(1-R_{1s}R_2)^2}\ , \tag{2.5}$$

and F is the *finesse* of the cavity. It is always optimum to arrange for $\delta_c=0$, corresponding to an isolated cavity being on resonance or maximum power buildup in a recycled system. With this choice, (2.4), simplies to

$$\frac{E_+}{E_0}=\frac{iT_{1c}T_{1s}R_2h_0\omega_L\sin(\omega\tau/2)e^{i\omega(t+\tau/2)}\left[e^{i(\delta_s-\omega\tau)}-R_{1s}R_2\right]}{\omega(1-R_{1c}R_2)(1-R_{1s}R_2)^2\{1+F_s'\sin^2[(\delta_s-\omega\tau)/2]\}}\ . \tag{2.6}$$

The expression contains virtually all of the information we need (for the other sideband, $\omega\rightarrow-\omega$). For example, the enhancement of the sideband amplitude by the choice of $\delta_s=\omega\tau$ (as in dual and detuned recycling) can be seen.

The sidebands are detected by beating them with a local oscillator field E_L to produce an intensity change ΔI:

$$\Delta I=(E_L+E_++E_-)(E_L^*+E_+^*+E_-^*)\ , \tag{2.7}$$

where an asterisk denotes complex conjugation. The fluctuating intensity δI is

$$\delta I=E_LE_+^*+E_LE_-^*+E_L^*E_++E_L^*E_-\ . \tag{2.8}$$

E_L may be an external field or may be some of the internal field which is allowed to leak out. For simplicity, we will take E_L to have the original laser frequency and to be in the quadrature phase (as an internal field would be). Insertion of (2.6) into (2.8) then gives, after some considerable algebra,

$$\begin{aligned}\delta I=&\frac{4E_0E_LT_{1c}T_{1s}R_2h_0\omega_L\sin(\omega\tau/2)}{\omega(1-R_{1c}R_2)(1-R_{1s}R_2)^2}\left[1+F_s'\sin^2\left[\frac{\delta_s+\omega\tau}{2}\right]\right]^{-1}\left[1+F_s'\sin^2\left[\frac{\delta_s-\omega\tau}{2}\right]\right]^{-1}\\&\times\left\{\sin\omega\left[t+\frac{\tau}{2}\right]\sin\omega\tau\left[\cos\delta_s+\left[\frac{2F_s^2}{\pi^2}\right](\cos\delta_s-\cos\omega\tau)\right]\right.\\&\left.+\cos\omega\left[t+\frac{\tau}{2}\right]\left[(\cos\delta_s\cos\omega\tau-R_{1s}R_2)\left[1+\frac{2F_s^2}{\pi^2}(1-\cos\delta_s\cos\omega\tau)\right]+\frac{2F_s^2}{\pi^2}\sin^2\delta_s\sin^2\omega\tau\right]\right\}\ .\end{aligned} \tag{2.9}$$

This expression gives the intensity change at the output of the interferometer as a function of the gravitational-wave frequency ω for any combination of detector parameters. In our investigation we shall need the *transfer function* $\tilde{K}(\omega)$ of the detector, which is defined as,

$$\tilde{\delta I}(\omega)=\tilde{K}(\omega)\tilde{h}(\omega)\ , \tag{2.10}$$

where a tilde denotes the Fourier transform and $\tilde{h}(\omega)$ is the Fourier transform of the signal. Taking the Fourier transform of Eq. (9) and performing lengthy algebra we get the following expression for the transfer function:

$$|\tilde{K}(\omega)|^2=I_0I_LR_2^2\mathcal{T}_c^2\mathcal{T}_s^2\left[\frac{\omega_L}{\omega}\right]^2\sin^2\left[\frac{\omega\tau}{2}\right]\frac{D}{M_+M_-}\ , \tag{2.11}$$

where

$$I_0=2|E_0|^2,\quad I_L=2|E_L|^2,\quad \mathcal{T}_c^2=\frac{T_{1c}^2}{(1-R_{1c}R_2)^2},\quad \mathcal{T}_s^2=\frac{T_{1s}^2}{(1-R_{1s}R_2)^2}\ . \tag{2.12}$$

$\mathcal{T}_c$ and $\mathcal{T}_s$ are the standard and dual *recycling factors*, respectively. Also,

$$M_\pm=1+F_s'\sin^2\left[\frac{\omega\tau\pm\delta_s}{2}\right]\ , \tag{2.13}$$

$$\begin{aligned}D=&1+F_s'\sin^2\left[\frac{\omega\tau}{2}\right]\cos\delta_s\\&+F_s'\sin^2\left[\frac{\delta_s}{2}\right]-\frac{\sin^2\delta_s}{(1-R_{1s}R_2)^2}\ .\end{aligned} \tag{2.14}$$

The spectral density $S_I(\omega)$ of the light intensity $\delta I(t)$ at the photodiode is given by the formula[1]

$$S_I=4\pi\frac{\hbar c}{\lambda_L}I_e\ , \tag{2.15}$$

where I_e is the rms intensity of the light at the photodiode, λ_L is the wavelength of the laser light, and $\hbar$ is Planck's reduced constant.

By formula (2.10), the spectral density $S_h(\omega)$, referred to the dimensionless amplitude of the gravitational wave,

is given by

$$S_h = 4\pi \frac{\hbar c}{\lambda_L} \frac{I_e}{|\tilde{K}|^2} . \tag{2.16}$$

In our case, where we assume that the light power on the photodiode is dominated by the local oscillator, $I_e = I_L$. Taking a quantum efficiency η of the photodiode, we get the following expression for S_h:

$$S_h(\omega) = \frac{1}{4\pi} \frac{\hbar \lambda_L}{\eta I_0 c} R_2^{-2} \mathcal{T}_c^{-2} \mathcal{T}_s^{-2} \frac{\omega^2}{\sin^2(\omega\tau/2)} \frac{M_+ M_-}{D} . \tag{2.17}$$

The above formula is a little complicated, but this is a result of its generality.

In Table I we summarize how one can obtain the spectral density $S_h(\omega)$ for particular configurations of the detector. We assume that each mirror has the same *losses* A^2, and we have the basic relation

$$R^2 + T^2 + A^2 = 1 , \tag{2.18}$$

where R and T are *amplitude* reflection and transmission coefficients, respectively. In the case of end mirrors, we have the relation

$$R_{\text{end}} = (1 - A^2)^{1/2} . \tag{2.19}$$

If we are recycling, the standard recycling factor can already be optimized independently of the signal, and we have the following optimum value for R_{1c}:

$$R_{1c\,\text{opt}} = R_2(1 - A^2) . \tag{2.20}$$

If cavities are used in the arms of the interferometer, then the recycling *mirrors* are also cavities. The transmission coefficients are then

$$T_{1c} = \frac{T_0 T_1}{1 - R_0 R_1} \left[1 + F_0' \sin^2 \frac{\delta_0}{2} \right]^{-1/2} , \tag{2.21}$$

$$T_{1s} = \frac{T_3 T_1}{1 - R_3 R_1} \left[1 + F_3' \sin^2 \frac{\delta_3}{2} \right]^{-1/2} , \tag{2.22}$$

where $F_0' = 4R_0R_1/(1-R_0R_1)^2$ and $F_3' = 4R_3R_1/(1-R_3R_1)^2$, $F_0 = (\pi/2)\sqrt{F_0'}$, $F_3 = (\pi/2)\sqrt{F_3'}$, and δ_0 and δ_3 are the *finesses* and offsets of the power recycling and signal recycling cavities, respectively.

If the interferometer cavity is run on resonance (as an isolated cavity), then the isolated recycling cavities should be off resonance (as an isolated cavity), then the isolated recycling cavities should be off resonance in order to behave as perfect mirrors, i.e.,

$$\delta_0 = \delta_3 = \pi .$$

In this case,

$$T_{1c} = \frac{T_0 T_1}{1 + R_0 R_1}, \quad T_{1s} = \frac{T_3 T_1}{1 + R_3 R_1} . \tag{2.23}$$

This allows the correct recycling mirror to be determined.

Only in detuned recycling are the (isolated) interferometer cavities run off resonance. If the power in the interferometer is to be kept high (i.e., $\delta_0 = 0$), the recycling cavity must then be operated nearly on resonance. However, this means that the power in the recycling cavity is greatly increased, thereby enhancing the significance of any losses there; our assumption that the losses are dominated by the cavity mirrors is probably unjustified in this case.[3,4] Since our analysis has shown that dual recycling has exactly the same shape of frequency response as detuned recycling, it would seem that dual recycling gives the best performance and greatest flexibility. Therefore, in the following we shall not consider detuned recycling any more.

TABLE I. Summary of the various parameter settings in general formula (10) in order to recover all possible detector configurations. These are determined by mirror reflectivities and cavity offsets. Note that, for recycled systems, an optimization of R_{1c} is assumed.

	Cavities $\tau = 2l/c$, $R_2 = (1-A^2)^{1/2}$	Delay lines $\tau = Nl/c$, $R_2 = (1-A^2)^{N/2}$
	No recycling	
	$R_{1c} = R_1$ $R_{1s} = R_1$ $\delta_s = 0$	$R_{1c} = 0$ $R_{1s} = 0$ $\delta_s = 0$
	Recycling $R_{1c\,\text{opt}} = R_2(1-A^2)$	
Standard recycling	$R_{1s} = R_1$ $\delta_s = 0$	$R_{1c} = R_0$ $R_{1s} = 0$ $\delta_s = 0$
Detuned recycling	$R_{1s} = R_1$	
Dual recycling	General Formula	$R_{1c} = R_0$ $R_{1s} = R_3$

III. APPROXIMATE ANALYTICAL FORMULAS

In the numerical analysis of signal-to-noise ratio presented in the following section, we have used the exact formula (2.17) for the spectral density of noise in the detector. However, for specific configurations of it, it is both possible and useful to obtain transparent analytical formulas which describe the frequency response of the antenna. We will summarize some of these formulas below.

A. No recycling

1. Cavities

For a nonrecycled detector using cavities in the arms, the noise spectral density takes on the form

$$S_h(\omega) = \frac{4\pi\hbar\lambda_L}{\eta I_0 c} f_c^2 \left[1 + \left[\frac{f}{f_c} \right]^2 \right] , \tag{3.1}$$

where the characteristic corner frequency f_c of the cavity is given by

$$f_c=\frac{(1-R_1R_2)c}{4\pi l} . \tag{3.2}$$

Here—and henceforth—we will use the frequency f rather than the angular frequency ω; they are related by $\omega=2\pi f$. We have assumed a detector size small compared with a gravitational wavelength, $2\pi fL/c \ll 1$, which is accurate for the proposed detectors.

2. Delay lines

For a nonrecycled detector using delay lines in the arms of the interferometer, the noise spectral density is

$$S_h(\omega)=\frac{\pi\hbar\lambda_L}{\eta I_0 c} f_d^2 \frac{(f/f_d)^2}{\sin^2(f/f_d)} , \tag{3.3}$$

where the characteristic frequency of the delay line is

$$f_d=\frac{c}{\pi N l} , \tag{3.4}$$

N being the *number of reflections* in the delay line.

B. Standard recycling

1. Cavities

If the optical losses are dominated by absorption and scattering at the cavity mirrors (of loss coefficient A^2), then the power buildup inside the recycling system is maximized, for any cavity, by choosing the recycling cavity to have a transmission $T_{1c}^2=2A^2$. This yields a spectral density

$$S_h(\omega)=\frac{\pi\hbar\lambda_L}{\eta I_0 c}\frac{cA^2}{\pi l} f_c\left[1+\left[\frac{f}{f_c}\right]^2\right] . \tag{3.5}$$

In this broadband operation mode, optimum sensitivity of the antenna to a given frequency $f=f_{\text{search}}$ is achieved by arranging mirror reflectivities so that $f_c=f_{\text{search}}$.

2. Delay lines

The power buildup within a delay line interferometer with N reflections is, if the losses are mainly at the delay line mirrors, optimized by choosing a recycling mirror transmission $T_0^2\approx NA^2$. This gives a noise spectral density of

$$S_h(\omega)=\frac{\pi\hbar\lambda_L}{\eta I_0 c}\frac{cA^2}{\pi l} f_d \frac{(f/f_d)^2}{\sin^2(f/f_d)} . \tag{3.6}$$

The minimum noise spectral density in this case occurs at $f\approx 1.2 f_d$.

C. Dual recycling

The frequency response of detectors using dual recycling is, in general, more complicated than those with no signal recycling. Good approximations to the frequency response may, however, still be found in special cases.

Two modes of operation may be distinguished: a *broadband* operation, where the signal recycling cavity is made resonant for the original laser frequency ($\delta_s=0$) and the bandwidth of the signal recycling cavity is comparable to the observing frequency, so that both signal sidebands are present; and a *narrow-band* operation, where the signal recycling cavity is tuned to one signal sideband ($\delta_s=\pm\omega\tau$), thereby allowing a high finesse, and so there is an efficient signal buildup at one frequency.

In the broadband mode, interferometers using cavities and delay lines with $f \ll f_d$ have the *same* frequency response: simply that given by (3.5) with $f_c=(2F_s\tau)^{-1}$.

In the narrow-band mode, detectors with cavities and delay lines *again* have the same response as long as $f \ll f_d$: If the bandwidth is fairly narrow, the spectral density of noise for a system tuned to f_0 is

$$S_h(\omega)=\frac{\pi\hbar\lambda_L}{\eta I_0 c}\left[\frac{cA^2}{4\pi l}\right]^2 \frac{(\pi\tau\Delta f)^2}{\pi\tau\Delta f - c\tau A^2/l} \times\left[1+4\left[\frac{f-f_0}{\Delta f^2}\right]^2\right] , \tag{3.7}$$

where

$$f_0=\frac{\delta_s}{2\pi\tau} , \tag{3.8}$$

$$\Delta f=\frac{1}{F_s\tau} . \tag{3.9}$$

Δf is the full width at half maximum (FWHM) bandwidth, and so the bandwidth is just the inverse of the signal *storage time.* Different transmissions of the signal recycling mirror give different signal storage times ($F_s\tau$) and so different sensitivity-bandwidth combinations. This is illustrated in Figs. 2 and 3. The minimum noise at the center frequency f_0 is obtained by choosing $2\pi\tau\Delta f=c\tau A^2/l$, $T_{1s}^2=2A^2$. The optimal detection of broadband signals, such as those from coalescing binaries, will require a somewhat broader bandwidth; the precise determination of the best combination of peak sensitivity, bandwidth, and tuning frequency will be the subject of Sec. V.

IV. GRAPHICAL ANALYSIS OF THE SENSITIVITY FUNCTION

In this section we give plots of the sensitivity function $\mathcal{S}(f)$, defined as the inverse of the spectral density $S_h(\omega)$. We have assumed that the length L of the arm is 3 km and that the losses in the mirrors are $A^2=5\times10^{-5}$.

In Figs. 2 and 3 we have considered cavities. In Fig. 2 we plot the sensitivity function for several values of the tuning frequency f_0, keeping transmission T_{1s} fixed. We find that the tuning of the signal recycling cavity determines the resonant frequency in accordance with formula (3.8). In Fig. 3 we plot the sensitivity function for the case of standard recycling and dual recycling with a fixed value of the frequency f_0. The function is plotted for several values of the transmission coefficient T_{1s} of the signal recycling cavity, and we find that the smaller the

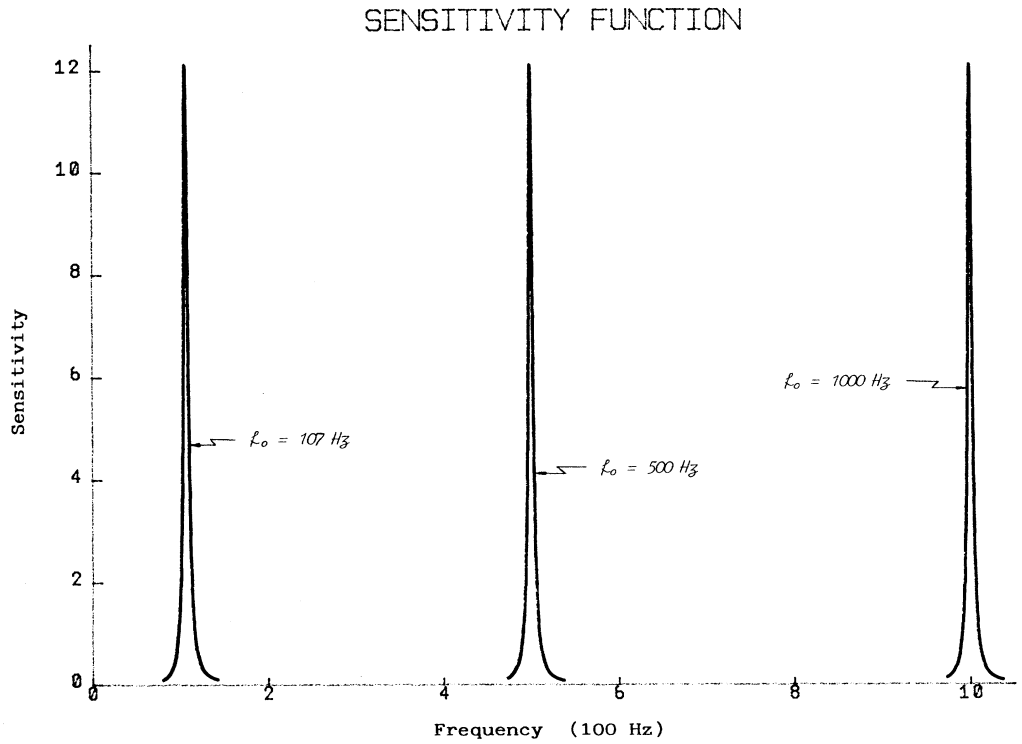

FIG. 2. Sensitivity function (in arbitrary units) vs frequency for narrow-band dual recycling implemented in a Fabry-Pérot interferometer. The effect of tuning the signal recycling cavities is shown for three values of the tuning frequency: $f_0=107$, 500, and 1000 Hz. The transmission of the signal recycling mirror has been chosen $T_{1s}^2=6\times10^{-4}$, whereby the FWHM bandwidth is $\Delta f=6.0$ Hz.

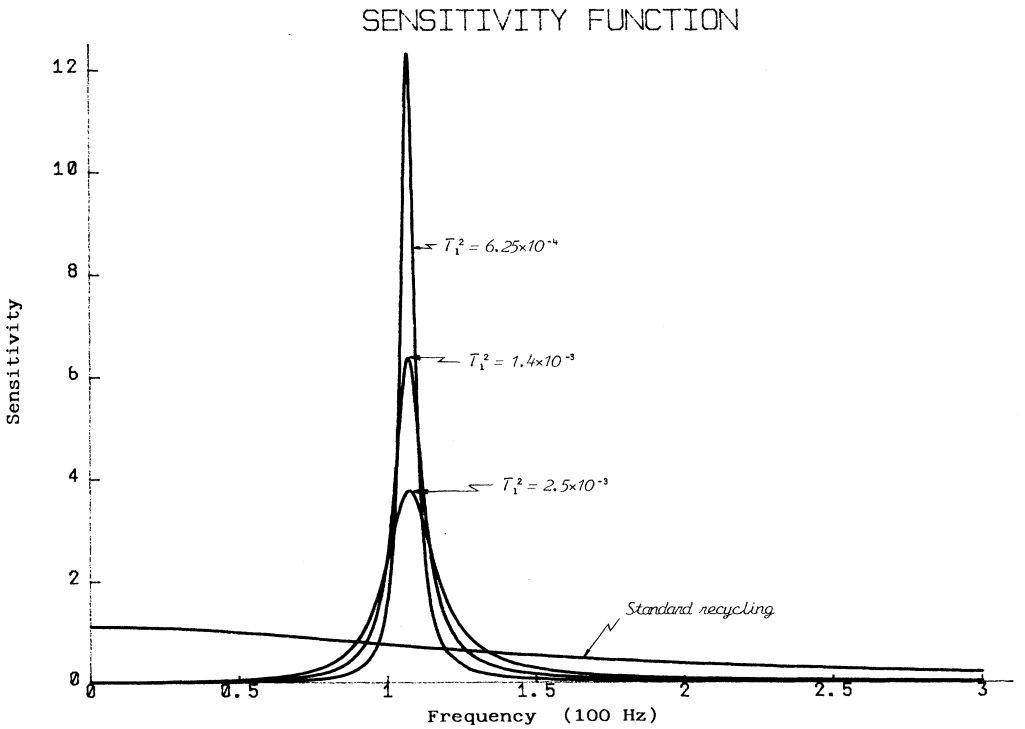

FIG. 3. Sensitivity function for the same device. In this case curves have been plotted for different values of the transmission of the signal recycling mirror with a fixed value of the tuning frequency $f_0=107$ Hz. The FWHM bandwidth increases with transmission—respective values are $\Delta f=6$, 12, and 21 Hz. Eventually, when no signal recycling is present ($T_{1s}^2=1$), one recovers the standard recycling sensitivity curve, which is also shown.

transmission of that cavity the narrower is the bandwidth, in accordance with the approximate general formula (3.9).

In Figs. 4 and 5 we have considered delay lines. In Fig. 4 we plot the sensitivity function for the case of standard recycling and that of broadband dual recycling ($\delta_s=0$) for several values of the transmission T_3 of the signal recycling mirror. In Fig. 5 we consider tuned dual recycling corresponding to 30 beam reflections within the delay lines. Plots are shown for a number of different values of the transmission coefficient T_3 of the signal recycling mirror and the tuning frequency f_0. We find that the smaller the transmission T_3, the narrower the bandwidth, in agreement with the approximate general formula (3.9). We also note that the offset of the signal recycling cavity (in this case made up of mirror M_3 and a delay line which can be considered as equivalent to a mirror with reflectivity R_2) determines the resonant frequency in accordance with formula (3.8).

V. OPTIMIZATION OF SIGNAL-TO-NOISE RATIO FOR COALESCING BINARIES IN A LASER INTERFEROMETER

To maximize the detectability of gravitational-wave signals in noise, we use optimal filtering. A standard result from the statistical theory of signal detection is that, if the noise is Gaussian, the filter that satisfies the Neyman-Pearson test is a linear filter whose Fourier transform is the Fourier transform of the signal divided by the spectral density of noise—see Ref. 9, Chaps. 3 and 4 for details. The Neyman-Pearson test is a test that maximizes detection probability subject to a certain chosen false-alarm probability.

The signal-to-noise ratio S/N that can be achieved with the optimum filter satisfies

$$(S/N)^2=2\int_0^\infty \frac{|\tilde{h}(f)|^2}{S_h(f)}df\ , \tag{5.1}$$

where $|\tilde{h}(f)|^2$ is the power spectrum of the signal. This is a most important parameter since it determines both the detection and false-alarm probability density functions. These are Gaussian distributions with *variance* equal to $(S/N)^2$ and with *mean* equal to $(S/N)^2$ and zero, respectively (Ref. 9, p. 119).

The characteristics of the gravitational-wave signal from coalescing binaries to post-Newtonian order have been investigated by one of us.[10,11] It was shown that for frequencies up to several hundred hertz the rms values of the gravitational-wave amplitudes to first post-Newtonian order are accurately described by the formulas quoted

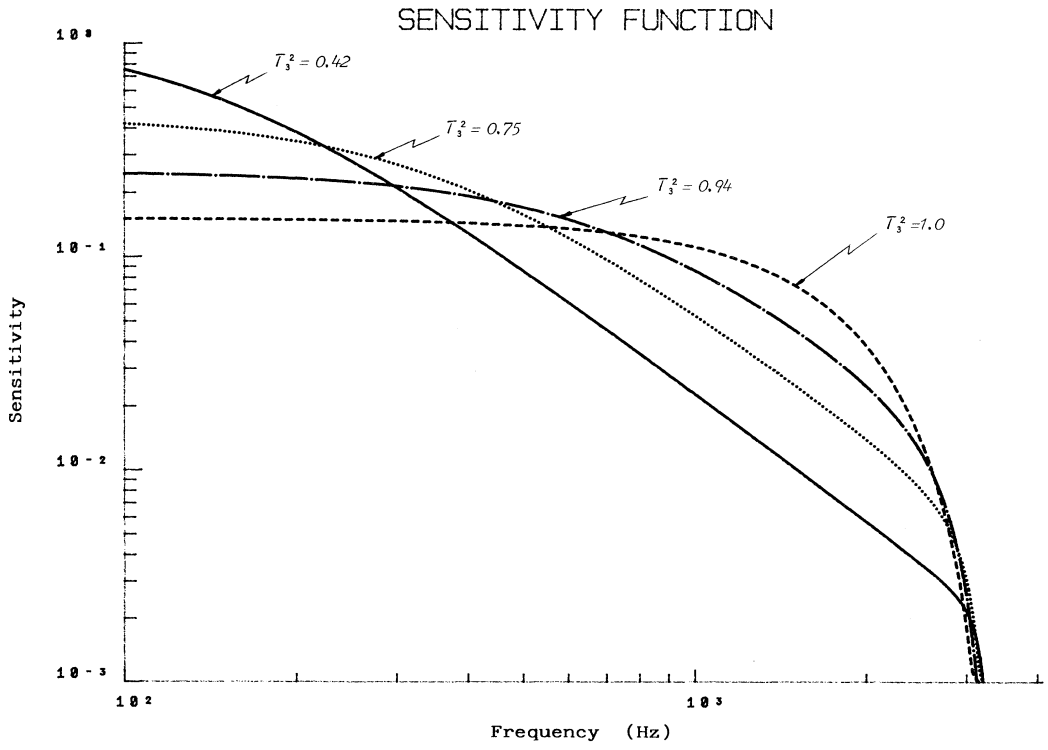

FIG. 4. Sensitivity function for broadband dual recycling in a delay line interferometer. The frequency offset is zero and 15 round trips of the laser beam have been assumed—the number of reflections in the mirrors is taken as $N=30$. Curves are provided for different transmission coefficients of the signal recycling mirror, including $T_3^2=1$, which corresponds to standard recycling.

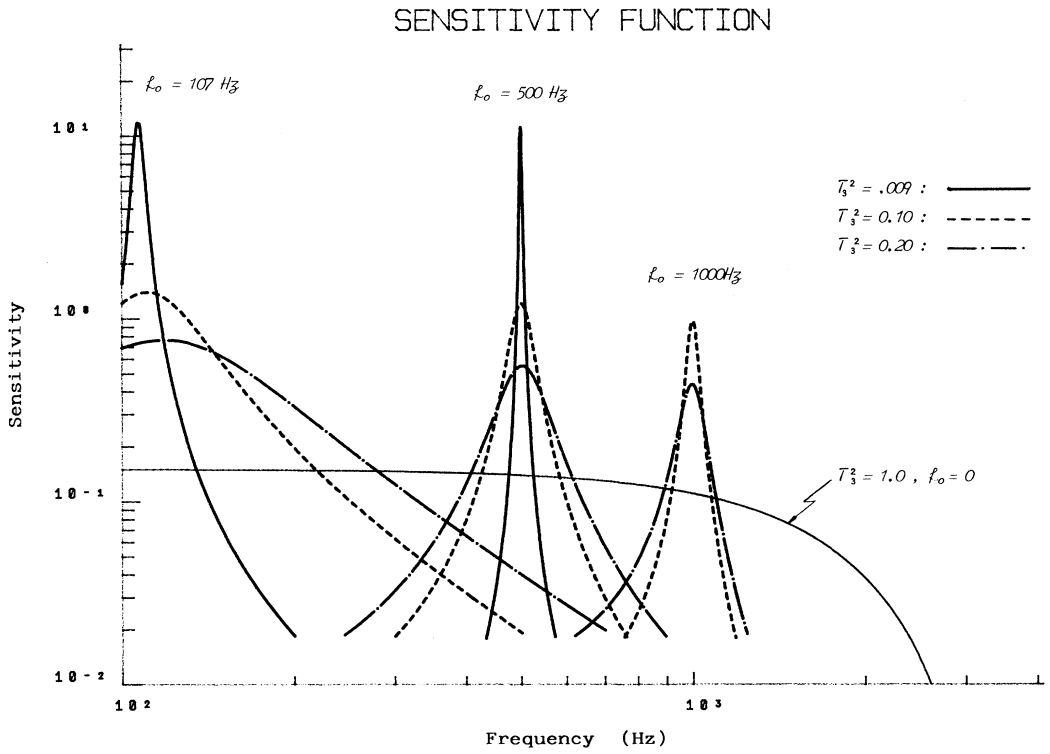

FIG. 5. Narrow-band dual recycling sensitivity function for a delay line interferometer. 30 beam reflections on the mirrors have been assumed again, and the effect of tuning the system for frequencies $f_0=107$, 500, and 1000 Hz is shown. Different curves are also provided to illustrate the effect of changing the transmission of the signal recycling mirror for each value of f_0. Standard recycling sensitivity is also represented for comparison.

below:

$$\langle h_1\rangle = 3.94\times10^{-25}\mu_\odot m_\odot f_{100} R_{100}^{-1}(\delta_{m_\odot}/m_\odot)\ , \tag{5.2}$$

$$\langle h_2\rangle = 1.02\times10^{-23}\mu_\odot m_\odot^{2/3} f_{100}^{2/3} R_{100}^{-1} \times[1-0.034(1-0.514\mu_\odot/m_\odot)(m_\odot f_{100})^{2/3}]\ , \tag{5.3}$$

$$\langle h_3\rangle = 9.15\times10^{-25}\mu_\odot m_\odot f_{100} R_{100}^{-1}(\delta m_\odot/m_\odot)\ , \tag{5.4}$$

$$\langle h_4\rangle = 3.24\times10^{-25}\mu_\odot (m_\odot f_{100})^{4/3} R_{100}^{-1}(1-3\mu_\odot m_\odot)\ . \tag{5.5}$$

The subscripts 1, 2, 3, and 4 in the amplitudes denote that they correspond to waves coming at 1, 2, 3, and 4 times the orbital frequency, respectively; $\mu_\odot$, $m_\odot$, and $\delta m_\odot$ are the reduced mass, total mass, and difference between masses of the components of the binary, expressed in units of the solar mass, respectively; f_{100} is *twice* the orbital frequency in 100 Hz, and R_{100} is the distance from the detector to the source in 100 Mpc. The dominant part of the amplitude $\langle h_2\rangle$ comes from the quadrupole radiation given by the standard quadrupole formula; the remaining terms in all the above formulas are post-Newtonian corrections. It should be remembered that the number of events within 100 Mpc is estimated to be about three per year.[12]

The above expressions for amplitudes correspond to rms averages over orientations of both source and detector, as well as over a period of the binary —see Ref. 11 for details. It is relevant at this point to note that, if one were lucky enough that the gravitational wave impinged on the detector in optimum orientation conditions, i.e., a wave vector orthogonal to antenna plane and linear polarization matching the interferometer's arms, then the above values would be increased by a factor of $\sqrt{5}$. While the averaged amplitude $\langle h_2\rangle$ is appropriate when considering coincident detection by a network, this possible enhancement of the amplitudes of the post-Newtonian components seen by a *single* antenna may significantly improve their detectability.

The characteristic time for the change of the period P of the binary, due to the radiation reaction, is given (in *seconds)* by

$$-\frac{\dot P}{P} = 7.97\mu_\odot^{-1} m_\odot^{-2/3} f_{100}^{-8/3}\left[1-0.030\left[1+\frac{1.24\mu_\odot}{m_\odot}\right]\times(m_\odot f_{100})^{2/3}\right]\ . \tag{5.6}$$

We expect that the shot-noise function $S_h(f)$—as given by Eq. (2.17)—will accurately represent the dominant

type of noise only above a certain frequency. Below it, other sources of noise (such as thermal and seismic noise) will be more important, and therefore Eq. (2.17) cannot be assumed to describe correctly the noise down to $f=0$. We will adopt the simplest model for low frequencies, namely, that the noise is infinitely large for frequencies below a certain cutoff f_s. Also, above another frequency, the tidal effects will start to influence the evolution of the binary system; this happens when one of the components of the binary fills its Roche lobe. Then, depending on the masses of the members of the system, the component that fills its Roche lobe either undergoes immediate tidal disruption or there is a flow of its mass through the Lagrange point to the other component.[13] According to the estimates of Clark and Eardly, for typical neutron-star binaries, this happens for orbital frequencies above 400 Hz—i.e., for dominant gravitational-wave signals above 800 Hz. Therefore, in our evaluation of signal-to-noise ratios, we shall also introduce an upper cutoff of 800 Hz.

To calculate the signal-to-noise ratio given by formula (5.1), we need to evaluate Fourier transforms of the gravitational waves with the amplitudes given above [formulas (5.2)–(5.5)]. In general, the gravitational-wave form $h(t)$ is given by

$$h(t)=A(f(t))\cos\left[2\pi\int^{t} f(t')dt'\right] . \tag{5.7}$$

In our case, for frequencies up to several hundred hertz, the frequency of the wave $f(t)$ is a slowly varying function of time. One can then use the following approximate formula for the modulus of the Fourier transform of $h(t)$:

$$|\tilde{h}(f)|\simeq A(f)/\sqrt{4\dot{f}} , \tag{5.8}$$

where the dot denotes a derivative with respect to time. In our case it is convenient to express $|\tilde{h}_I|$ in the following form, where I stands for number of orbital frequencies:

$$|\tilde{h}_I|=\langle h_1\rangle\sqrt{P/4f} . \tag{5.9}$$

Using the latter formulas and the expression for the spectral density of noise in the interferometer, given in Sec. II, we obtain the following results for signal-to-noise ratios corresponding to various gravitational wave amplitudes [subscripts in $(S/N)^2$ correspond to subscripts in the average amplitudes $\langle h_1\rangle$]:

$$(S/N)_1^2=\left[0.25A_0\frac{\delta m_\odot}{m_\odot}\frac{\mu_\odot^{1/2}m_\odot^{2/3}}{R_{100}}\right]^2\frac{J_3}{f_{s_{100}}^{8/3}} , \tag{5.10}$$

$$(S/N)_2^2=\left[12.09A_0\frac{\mu_\odot^{1/2}m_\odot^{1/3}}{R_{100}}\right]^2\frac{J_2}{f_{s_{100}}^{10/3}} , \tag{5.11}$$

$$(S/N)_3^2=\left[1.71A_0\frac{\delta m_\odot}{m_\odot}\frac{\mu_\odot^{1/2}m_\odot^{2/3}}{R_{100}}\right]^2\frac{J_3}{f_{s_{100}}^{8/3}} , \tag{5.12}$$

$$(S/N)_4^2=\left[0.38A_0\frac{\mu_\odot^{1/2}m_\odot^{1/3}}{R_{100}}\right]^2\frac{J_4}{f_{s_{100}}^{2}} , \tag{5.13}$$

where $f_{s_{100}}$ is the frequency cutoff in 100 Hz and

$$A_0=\left[\frac{0.514\ \mu\text{m}}{\lambda_L}\right]^{1/2}\left[\frac{\eta I_0}{50\ \text{W}}\right]^{1/2} , \tag{5.14}$$

$$J_n=R_2^2\mathcal{T}_{c\,\text{opt}}\mathcal{T}_s\int_{f_{s_{100}}}^{8}\sin^2(\pi f_{100}\tau_{-2})\frac{D}{M_+M_-}\frac{df_{100}}{f_{100}^{(17-2n)/3}} . \tag{5.15}$$

Here $M_\pm$ and D are given by formulas (2.13) and (2.14), and we have written $\omega\tau/2\equiv\pi f_{100}\tau_{-2}$, with f_{100} the signal's frequency in 100 Hz and τ_{-2} given in hundredths of a second. $\mathcal{T}_{c\,\text{opt}}$ is the maximum value of the recycling factor, given by $R_{1c}=R_2(1-A^2)$—cf. Sec. II above. For a 3-km antenna, it is hoped that the thermal noise will be less than photon-counting noise for frequencies above 100 Hz. There should also be sufficient seismic isolation for such range of frequencies. We therefore set $f_{s_{100}}=1$ for the coming discussion.

We have investigated the integrals (5.10)–(5.13) numerically for all the configurations of the laser interferometer. For each configuration we have found values of the parameters of the detector that maximize the signal-to-noise ratio in each case. In Table II we give a summary of our results.

In the parameter entries to that table we have added (where appropriate) the bandwidth parameter Δf, the inverse of the signal's storage time (cf. Sec. III):

$$\Delta f=\frac{1}{F_s\tau} . \tag{5.16}$$

In a narrow-band configuration, Δf is the FWHM bandwidth; in broadband operation, Δf is still a measure of bandwidth—it is the frequency at which the signal falls by a factor of $\sqrt{5}$. In this case, Δf is equal to the cavity linewidth, which is twice Thorne's "knee frequency."[1] As we shall see, Δf is especially suited for the representations of signal-to-noise ratio contour maps.

As can be seen in Table II, maxima for delay lines occur for very high values of N, the number of beam reflections in the mirrors. This is a mathematical property of our $(S/N)^2$ integrals, but these maxima are physically impracticable—huge mirrors would be needed to enable such numbers of beams in the interferometer's arms. A sensible value for N, according to the British-German proposal to build a detector,[8] is around $N=30$. In Table III we give the values of the antenna parameters f_0 and Δf which maximize the $(S/N)^2$ integral for a *fixed* $N=30$, along with the corresponding value of the integral. It is remarkable that the latter very closely approach the optima obtained for narrow-band dual recycling for a Fabry-Pérot interferometer—cf. the respective rows in Tables II and III. In Table IV we give actual signal-to-noise ratios for two binary systems, which can be considered as plausible examples of the ones expected in practice. It is interesting to note that, by making the detector narrow banded, an improvement in the signal-to-noise ratio of between 1.5 and 2 is obtained for all coalescing binary signals. This is a general property of the signal and noise power spectra we are dealing with. A proof of this general result is given in the Appendix.

TABLE II. Comprehensive description of optimum antenna performance for all configurations considered in this paper and all components (Newtonian and post-Newtonian) of radiation form a coalescing binary-star system. Results are presented as the values of the signal-to-noise ratio integrals J_I ($I=2,3,4$) in formulas (5.15)—see also (5.10)—and (5.13) in the text. Figures have been obtained by means of computer-aided numerical analysis. Note that no maximum has been found for J_4 and dual recycling in Fabry-Pérot interferometers, hence the vacancy in the corresponding entries. This means that making the detector narrow banded in dual recycling can produce no improvement over standard recycling when applied to optimize detection of h_4 with a Farby-Pérot antenna.

	Optimal parameter values			Integrals		
Configuration	J_2	J_3	J_4	J_2	J_3	J_4
Cavities						
No recycling	$R_1=0.9977$ $\Delta f=37$	$R_1=0.9976$ $\Delta f=39$	$R_1=0.9975$ $\Delta f=40$	0.007	0.009	0.012
Standard recycling	$R_{1s}=0.982$ $\Delta f=290$	$R_{1s}=0.980$ $\Delta f=321$	$R_{1s}=0.977$ $\Delta f=376$	0.32	0.42	0.62
Dual recycling	$R_{1s}=0.9997$ $f_0=107$ $\Delta f=6$	$R_{1s}=0.9996$ $f_0=108$ $\Delta f=7$	No Max.	0.78	0.83	No Max.
Delay lines						
No recycling	$N=375$	$N=359$	$N=341$	0.006	0.008	0.010
Standard recycling	$N=237$ $N=467$	$N=211$ $N=457$	$N=176$ $N=442$	0.42	0.54	0.75
Dual recycling	$R_{1s}=0.937$ $f_0=107$ $\Delta f=5$	$R_{1s}=0.930$ $f_0=109$ $\Delta f=6$	$R_{1s}=0.919$ $f_0=113$ $\Delta f=7$	1.23	1.32	1.46

Entries in Table IV correspond to optimum performance of the detector with respect to the various components of radiation, i.e., h_1, h_2, h_3, or h_4, *independently*. In practice, however, one will have to make a choice as to which is the kind of signal one wants the detector to be most sensitive to—since optimum tuning for all four at the same time is impossible. So a question suggests itself immediately: If the detector is optimized for h_2 (no doubt the most sensible choice to begin with), how good is its performance to sense h_1, h_3, and h_4? The answer to such question is that it will not vary too much from the values in the tables above, the reason being that, in each case, maxima occur for like values of the parameters. For example, if we tune the interferometer to have the maximum $(S/N)_2^2$ with dual recycling ($N=30$), then sensitivity goes down by only 1.2% and 1.3%, respectively, for h_1 and h_3 and h_4 with respect to their maximum values in Table IV. A detailed search of all the possibilities shows that degradation in the signal-to-noise ratio for post-Newtonian components by tuning the antenna to the Newtonian is always below 2%.

In a set of figures we have shown contour maps of the signal-to-noise ratio integral J_2 of a Newtonian chirp. In Fig. 6 we have shown the isoheight contours of J_2 for a Fabry-Pérot interferometer in terms of the parameters f_0 and Δf. Note the existence of a quite sharply peaked maximum corresponding to a narrow-band system tuned to a frequency just above the seismic cutoff f_s. This may be interpreted as being the result of concentrating the region of good sensitivity at a frequency where the power in the signal is high. There is also a lower and smoother maximum for $f_0=0$, $\Delta f=290$ Hz, which corresponds to standard recycling.

In Figs. 7–10 we have presented contour plots of J_2 for recycled delay lines. Since the signal-to-noise ratio in this case depends on *three* parameters—number of reflections of the laser light within each interferometer's arm and frequencies f_0 and Δf—we have shown three

TABLE III. Optimal values in Table II for delay lines occur for very high values of the parameter N. In this table we give a more realistic account of the interferometer's performance by taking $N=30$. For dual recycling a search has been pursued in the $(f_0,\Delta f)$ plane for that particular value of N.

	Optimal parameter values			Integrals		
Configuration	J_2	J_3	J_4	J_2	J_3	J_4
No recycling	($N=30$)	($N=30$)	($N=30$)	0.0002	0.0003	0.0005
Standard recycling	($N=30$)	($N=30$)	($N=30$)	0.10	0.16	0.30
Dual recycling	($N=30$) $f_0=107$ $\Delta f=6$	($N=30$) $f_0=108$ $\Delta f=7$	($N=30$) $f_0=111$ $\Delta f=8$	0.77	0.82	0.88

TABLE IV. Actual signal-to-noise ratios for two plausible examples of coalescing binary systems. Entries corresponding to delay line interferometers have been chosen to be optimum but compatible with the restriction $N=30$. A most remarkable result is that narrow-band dual recycling produces, for this value of N, almost identical signal-to-noise ratios as it does in a Fabry-Pérot interferometer, whenever the latter is set to work at its best efficiency.

Gravitational-wave amplitude	Signal-to-noise ratio: Cavities NR	Cavities SR	Cavities DR	Delay lines NR	Delay lines SR	Delay lines DR
			$m_{2\odot}=m_{1\odot}=1.4$			
$\langle h_1 \rangle$	0	0	0	0	0	0
$\langle h_2 \rangle$	1.2	8.1	12.6	0.20	4.5	12.5
$\langle h_3 \rangle$	0	0	0	0	0	0
$\langle h_4 \rangle$	0.05	0.35		0.01	0.13	0.22
			$m_{2\odot}=m_{1\odot}/3=1$			
$\langle h_1 \rangle$	0.03	0.2	0.25	0.004	0.11	0.22
$\langle h_2 \rangle$	1.4	9.4	14.6	0.20	5.2	14.5
$\langle h_3 \rangle$	0.02	1.2	1.7	0.03	0.73	1.6
$\langle h_4 \rangle$	0.06	0.40		0.009	0.29	0.46

corresponding cross sections of J_2, successively associated with holding N, f_0, and Δf fixed. Thus, in Fig. 7, we have given the cross section associated with $N=30$, which, as discussed above, constitutes a realistic example (rather than the enormous $N=467$ in Table II). In Fig. 8 we hold fixed $f_0=107$ Hz, here one can see two peaks (like in Fig. 6), the sharper of the two corresponding to the maximum reported in Table II. Figure 9 also has f_0 fixed ($f_0=0$) and, thus, the antenna operating in broadband dual recycling. Finally, in Fig. 10 we keep Δf constant and again two maxima appear, at almost the same value of f_0. These last figures are basically illustrative, since one does not expect to have in practice much freedom to choose the parameter N, the number of reflections. However, the value of N, together with our assumed arm length of 3 km, may be taken as indicating a storage time for the delay lines. Thus apparently large values of N may one day become accessible if much larger detectors are ever contemplated. This combined set of figures allows signal-to-noise ratios to be read off for essentially any detector configuration.

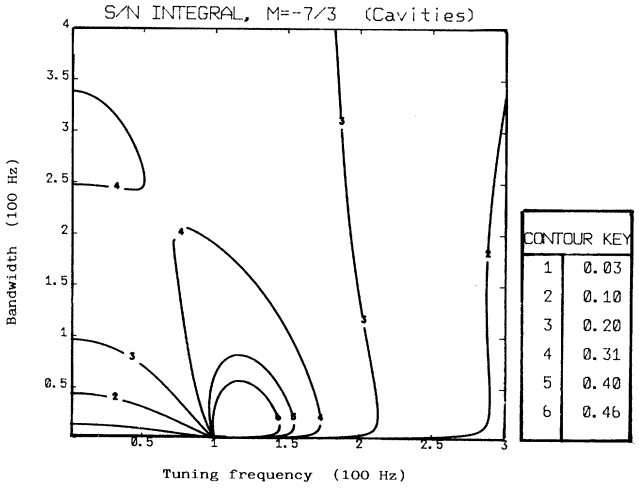

FIG. 6. Contour map of the signal-to-noise ratio integral. J_2—cf. formula (5.15) in the text—for the Newtonian component of the radiation emitted by a coalescing binary-star system. The interferometer is operated in dual recycling and the arms are assumed to be Farby-Pérot cavities; frequencies are given in 100 Hz. Note a maximum at $f_0=0$ corresponding to standard recycling.

VI. CONCLUSION

In this paper we have discussed the detectability of the gravitational radiation from coalescing compact binary

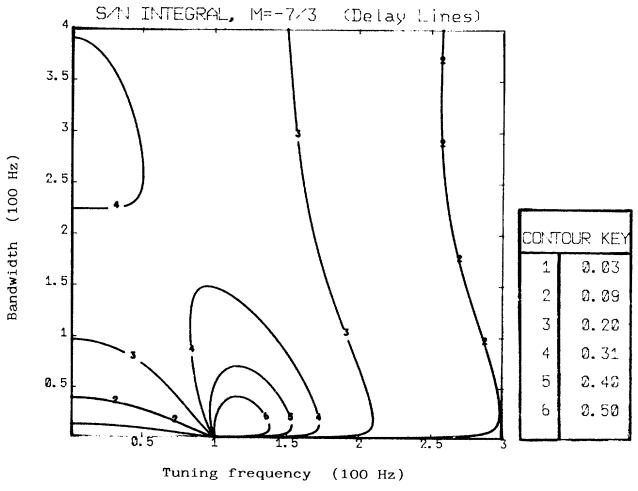

FIG. 7. Same as before, except that delay line arms are now assumed. The map corresponds to $N=30$—rather than the mathematical optimum $N=467$. It very much resembles the previous one, which means that performance is quite similar for these two configurations of the antenna.

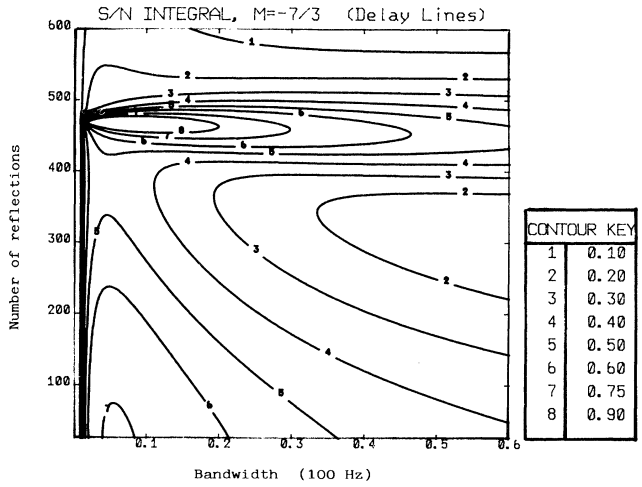

FIG. 8. Signal-to-noise ratio integral J_2 for delay line interferometers with dual recycling for a fixed value of the tuning frequency set to $f_0=107$ Hz. The maximum reported in Table II can be seen along with another one for $N=30$—cf. Table III. The N-axis range stretches from $N=25$ to 600.

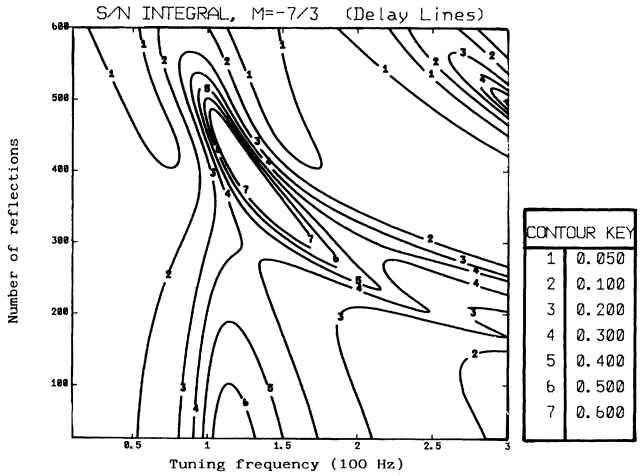

FIG. 10. Last remaining possibility: We hold fixed the detector's bandwidth and plot J_2 in terms of f_0 and N. Because of extremely abrupt slopes, however, the map corresponds to $\Delta f=30$ Hz rather than to the 5 Hz of Table II. Qualitative features are kept after this change, though. Note once more the presence of two peaks, one of which corresponds to a very high value of N, the other lying on the lower boundary of this parameter's range.

systems by the new generation of proposed laser interferometers. We have seen that long detectors with fairly high laser powers, using light recycling, will be necessary in order to achieve reliable detection, but that quite good signal-to-noise ratios are possible with such a system. Thus, a 3-km interferometer with 50 W of effective power, using broadband recycling with the parameters assumed earlier, will see the coalescence of a binary system consisting of two $1.4M_\odot$ neutron stars at a distance of 100 Mpc with a signal-to-noise ratio, *on average,* of about 10. With fortunate orientation, this number can be as high as 20 in a *single* detector.

Furthermore, making the detector narrow banded with dual recycling and matching the region of good sensitivity to the region of high signal power may give a significant improvement in signal-to-noise ratio. For the 3-km interferometer that we have taken as our example, the optimum bandwidth is about 6 Hz—twice the optimum for periodic signals. This gives an improvement in signal-to-noise ratio, compared to a broadband system, of a factor of ~ 1.5. Alternatively, the volume of space that becomes observable by the narrow-band system is larger by a factor of ~ 3.5.

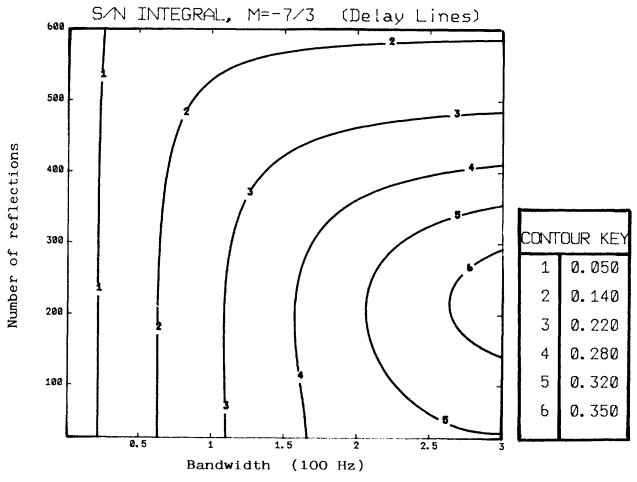

FIG. 9. Same graph, but with no frequency offset ($f_0=0$). No maximum can be seen—the slope continues indefinitely (but very smoothly) beyond the right margin of the viewpoint region.

The Newtonian component of the radiation for our $1.4M_\odot$ neutron-star binary at 100 Mpc would give an average signal-to-noise ratio of ~ 12 for our optimized narrow-band detector. Signal-to-noise ratios for other combinations of sensitivity and bandwidth may be read off the contour plots (Figs. 6–9) and formulas (5.10)–(5.13) above.

Another question we have addressed in this paper is whether the post-Newtonian components of the gravitational radiation that occur at different harmonics of the orbital frequency can be detected. Observation of odd harmonics would allow the masses of the individual precursor objects to be measured, rather than just a combination of their masses—this is especially important if we are trying to confirm an observation of a black hole. We have shown that the gain in signal-to-noise ratio derived from making the detector narrow banded is comparable for all post-Newtonian components and the Newtonian one, despite their somewhat different frequency spectra. Furthermore, the optimum combination of detector tuning, sensitivity, and bandwidth is negligibly different for the different components. Nevertheless, observation of the post-Newtonian components from typical binary systems looks difficult—cf. Table IV. This is despite the fact that observation of the Newtonian com-

ponent by a network of antennas, with the resultant deduction of a direction, arrival time, and mass parameter, will severely constrain the possible arrival times of the post-Newtonian component, thus lowering the threshold for detection. The most promising post-Newtonian component for observation may well be the third harmonic. For example, a binary system consisting of a $5M_\odot$ black hole and a $1.4M_\odot$ neutron star at 100 Mpc would produce an *average* signal-to-noise ratio in our narrow-band detector of 3.1, which would be adequate for confident detection (the Newtonian component of such a system would be seen with an average signal-to-noise ratio of 21). Allowing for the presence of four detectors in the network (or a single fortunately oriented one) would improve the effective signal-to-noise ratio by another factor of 2, giving a measurement of $\delta m_\odot/m_\odot$ for this system to $\sim 15\%$. This would clearly indicate the presence of a black hole.

The discussion here has concentrated on the possible signal-to-noise ratio produced by the gravitational waves. Moreover, if a world wide network of detectors is to be used as an astrophysical observatory, it is also important to be able to measure the characteristics of the signal—i.e., amplitude, direction, sweep rate, etc.—as accurately as possible. While this problem has already been examined, a thorough treatment for all detector configurations is still lacking. We plan to discuss this in future publications.

ACKNOWLEDGMENTS

A.K. would like to acknowledge financial support from CSIC, Spanish Ministry of Education. J.A.L. also acknowledges Spain's Ministry of Education for financial help provided via Contract No. PS87-0046 and Spain's and Poland's Ministries of Foreign Affairs for funding a 2-week visit to the Polish Academy of Sciences. B.J.M. would like to acknowledge support from the Royal Society, the Science and Engineering Council, and the University of Glasgow.

APPENDIX A

We want to show in this appendix that, by making an interferometric gravitational-wave detector narrow banded, one can achieve an improvement in signal-to-noise ratio which is of the order of $\sqrt{2}$ over optimum broadband signal-to-noise ratio for the detection of coalescing binary signals ("chirps"). We shall take the broadband configuration to be standard recycling and the narrow-band configuration to be either detuned recycling or narrow-band dual recycling—both have the same sensitivity functions.

To do so we will estimate the value of the ratio

$$\frac{(S/N)^2_{\rm NB}}{(S/N)^2_{\rm BB}}\ , \tag{A1}$$

for optimum performance in each case, and find out it is of the order of 2. To estimate $(S/N)^2_{\rm NB}$ is not very difficult: If the bandwidth is quite narrow, one can easily prove that

$$\left[\frac{1}{S_h(f)}\right]_{\rm NB} \sim \frac{\pi}{4}\delta(f-f_0)\ , \tag{A2}$$

whenever the bandwidth Δf approaches zero; this result is obtained upon simple analysis of expression (3.7) in the text. If we replace this approximate formula into (5.1), we immediately obtain

$$(S/N)^2_{\rm NB} \sim \frac{\pi}{4}|\tilde{h}(f_0)|^2\ , \tag{A3}$$

thereby getting $(\pi/4)f_0^{-7/3}$ as an approximation to $(S/N)^2$ for a Newtonian chirp [except for a common coefficient which cancels in (A1)].

We next look at the value of $(S/N)^2$ for broadband operation mode. It is far less simple in this case to arrive at a concise result like before. For now, integrals of the type (5.1) are not easy to estimate because of contributions to their value of complicated functions over considerably long independent variable intervals. In addition, one must find a value of Δf [or, indeed, f_d in formula (3.6)] which maximizes the result. Numerical analysis of this process, however, can almost be made with a pocket calculator, the final result being that displayed in Table II.

Accepting that value, one finds

$$\frac{(S/N)^2_{\rm NB}}{(S/N)^2_{\rm BB}} \sim 2.10\ . \tag{A4}$$

This is a number very close to 2, and so improvement in signal-to-noise ratio is very nearly $\sqrt{2}$, as announced above.

[1]K. S. Thorne, in *300 Years of Gravitation,* edited by S. W. Hawking and W. Israel (Cambridge University Press, Cambridge, England, 1987), pp. 330–458.

[2]R. W. P. Drever, in *Gravitational Radiation,* edited by N. Dervelle and T. Piran (North-Holland, Amsterdam, 1983), pp. 321–338.

[3]J.-Y. Vinet, B. Meers, C. N. Man, and A. Brillet, Phys. Rev. D **38**, 433 (1988).

[4]B. J. Meers, Phys. Rev. D **38**, 2317 (1988).

[5]B. J. Meers, Phys. Lett. A **142**, 465 (1989).

[6]Sheryl Smith, Phys. Rev. D **36**, 2901 (1987).

[7]S. V. Dhurandhar, A. Krolak, and J. A. Lobo, Mon. Not. R. Astron. Soc. **238**, 1407 (1989).

[8]J. Hough, B. J. Meers, G. P. Newton, N. A. Robertson, H. Ward, G. Leuchs, T. M. Niebauer, A. Rüdinger, R. Schilling, L. Schnupp, H. Walther, W. Winkler, B. F. Schutz, J. Ehlers,

P. Kafka, G. Schäfer, M. W. Hamilton, I. Schütz, H. Welling, J. R. J. Bennett, I. F. Corbett, B. W. H. Edwards, R. J. S. Greenhalgh, and V. Kose, Max Plank Institut für Quantenoptik, Garching, Munich, Germany, Report No. MPQ and Report No. 147 GWD/137/JH(89), 1989 (unpublished).

[9]C. W. Helstrom, *Statistical Theory of Signal Detection* (Pergamon, Oxford, 1968).

[10]A. Krolak and B. F. Schutz, Gen. Relativ. Gravit. **19**, 1163 (1987).

[11]A. Krolak, in *Gravitational Wave Data Analysis,* edited by B. F. Schutz (Reidel, Amsterdam, 1989), pp. 59–69.

[12]B. F. Schutz, Class. Quantum Grav. **6**, 1761 (1989).

[13]J. P. A. Clark and D. M. Eardley, Astrophys. J. **215**, 311 (1977).